
A CAUSAL CONVOLUTIONAL NEURAL NETWORK FOR MOTION MODELING AND SYNTHESIS

A PREPRINT

Shuaiying Hou Zhejiang University China 11721044@zju.edu.cn	Weiwei Xu* Zhejiang University China xww@cad.zju.edu.cn	Jinxiang Chai Texa A&M University USA jchai@cs.tamu.edu	Congyi Wang Xmov China artwang007@gmail.com
Wenlin Zhuang Southeast University China wlzhuang@seu.edu.cn	Yu Chen Xmov China chenyu@xmov.ai	Hujun Bao Zhejiang University China bao@cad.zju.edu.cn	Yangang Wang Southeast University China yangangwang@seu.edu.cn

February 1, 2021

ABSTRACT

We propose a novel deep generative model based on causal convolutions for multi-subject motion modeling and synthesis, which is inspired by the success of WaveNet in multi-subject speech synthesis. However, it is nontrivial to adapt WaveNet to handle high-dimensional and physically constrained motion data. To this end, we add an encoder and a decoder to the WaveNet to translate the motion data into features and back to the predicted motions. We also add 1D convolution layers to take skeleton configuration as an input to model skeleton variations across different subjects. As a result, our network can scale up well to large-scale motion data sets across multiple subjects and support various applications, such as random and controllable motion synthesis, motion denoising, and motion completion, in a unified way. Complex motions, such as punching, kicking and, kicking while punching, are also well handled. Moreover, our network can synthesize motions for novel skeletons not in the training dataset. After fine-tuning the network with a few motion data of the novel skeleton, it is able to capture the personalized style implied in the motion and generate high-quality motions for the skeleton. Thus, it has the potential to be used as a pre-trained network in few-shot learning for motion modeling and synthesis. Experimental results show that our model can effectively handle the variation of skeleton configurations, and it runs fast to synthesize different types of motions on-line. We also perform user studies to verify that the quality of motions generated by our network is superior to the motions of state-of-the-art human motion synthesis methods.

Keywords Deep learning · Temporal convolutional neural network · Motion synthesis and control · Optimization · Motion denoising · Motion completion

1 Introduction

It is a challenging task to learn a powerful generative motion model from prerecorded human motion data because human motion is intrinsically governed by highly nonlinear dynamical systems. An appealing solution for generative motion models should scale up well to motion datasets across multiple subjects. In addition, it should be accurate and compact, efficient for runtime evaluation, and amenable to various forms of applications, such as motion synthesis with or without control inputs, motion prediction, motion denoising, and motion completion.

*corresponding author

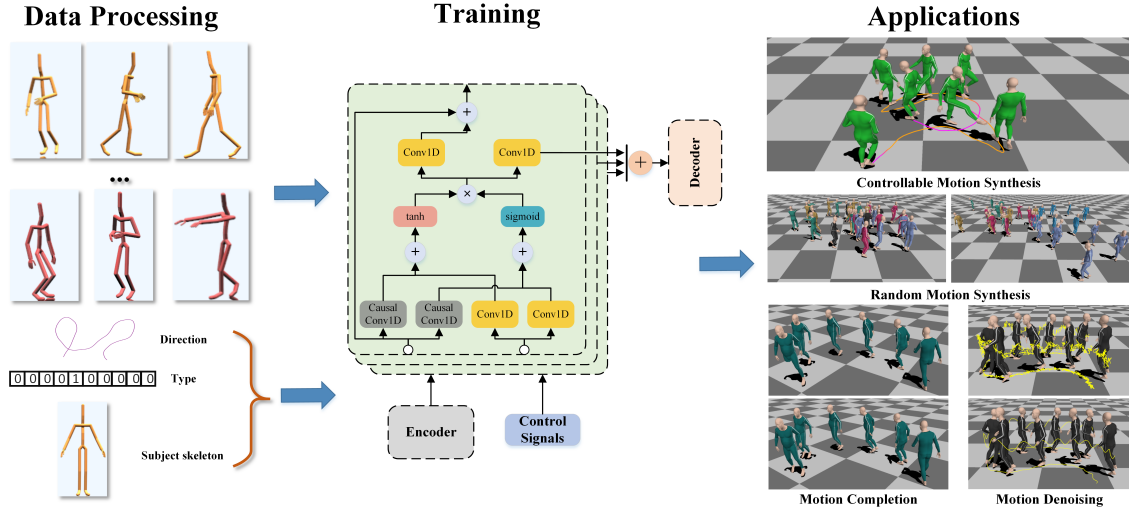


Figure 1: Our causal convolutional neural network can scale up well to a large-scale motion dataset across multiple subjects and support a variety of applications, as listed in this figure, in a unified way with a single set of network parameters. Left: Examples of motion capture data. Middle: Training of our network. Right: Applications.

Recent deep learning-based motion synthesis algorithms show great potentials in resolving these issues. The deep neural network with nonlinear activation functions can well model nonlinear dynamics and generate different motions without the motion capture data used for network training to save the memory footprint. Autoregressive models, such as restricted Boltzmann machines (RBMs) and recurrent neural networks (RNNs) [1, 2, 3], have been applied to motion synthesis by predicting the possibility of motions in the future. However, to avoid causal error accumulation in such models, careful training strategies must be employed. Conditioned on control signals, convolutional neural networks (CNN), phase-functioned neural network (PFNN), Long-short term memory (LSTM) networks, and variational autoencoders have been applied to generate controllable motions to interact with the environment for a specific person [4, 5, 6, 7]. Despite significant progress in deep learning-based motion modeling, there is no accurate generative model that can scale up well to motion datasets across multiple subjects and support different applications in a unified way.

This paper proposes a novel causal convolutional neural network (CCNet) to address the aforementioned issues in generative motion modeling and synthesis. The network architecture is inspired by the success of causal-convolution-based WaveNet [8] in multi-subject speech synthesis. The causal convolution is appealing to generative human motion modeling since it can explicitly model the correlation among a long-range temporal window, which is demonstrated to be more effective than the hidden states used in RNNs and their variations in speech synthesis experiments. However, it is a non-trivial task to apply WaveNet to motion synthesis because motion data is a high dimensional signal, and one needs to pay attention to foot contact to synthesize plausible motions. To this end, we adapt the network architecture of the WaveNet by adding an encoder and a decoder to translate the motion data into features and back to the predicted motions. Moreover, we add 1D convolution layers to allow the CCNet to take skeleton configurations as an input, which is critical for the network to handle the skeleton variations of different subjects. The output of the CCNet is the probabilistic density function (PDF) of the motion at the next time step that is conditioned on the motions at previous time steps, control signals, and the skeleton configuration. Consequently, with a meticulously-designed training strategy, our CCNet can capture personalized style variation of different skeletons and effectively support random and controllable motion synthesis in a unified way using a single set of network parameters.

The CCNet possesses the desirable properties of the generative motion model. It is a compact model of size ~ 4.5 M bytes. Combined with a Gaussian loss that penalizes the deviation of joint angles, positions, and velocities simultaneously in training, the drifting or freezing issues that are frequently encountered in RNN models can be effectively mitigated. Thus, the CCNet can be applied to random motion synthesis, i.e., synthesizing long-time motion sequences of different subjects without control signals. This renders it suitable for motion generation, denoising, and completion applications. The CCNet can also be applied to the controllable motion synthesis. After training on the motion capture (mocap) data across multi-subjects, we allow the user to control the motion synthesis result through various control signals, such as heading direction, velocity, and motion type. The skeleton is also called control signals hereafter and processed in the same way as other control signals in the CCNet. Moreover, the CCNet can synthesize motions for novel skeletons not in the training dataset. After fine-tuning the network with a few motion data of the novel skeleton, it is able to capture

Methods	Generative Model		Scalability	Applications					Motion Quality
	I	II		I	II	III	IV	V	
MotionGraph[22] [23][17]	×	×	×	✓	✓	×	×	×	✓
MotionGraph++[21]	o	o	×	✓	✓	×	×	×	✓
ERD-LSTM[2] [6] [3] [24]	✓	✓	o	✓	o	o	✓	✓	o
DAE-LSTM[25]	✓	✓	o	o	✓	o	o	o	✓
PFNN[5]	✓	✓	✓	-	✓	-	-	-	✓
CCNet	✓	✓	✓	✓	✓	✓	✓	✓	✓

Table 1: Comparisons between the CCNet and state-of-the-art deep-learning-based models in motion modeling and synthesis. Columns I, II of "generative model" are the model size and motion variation during synthesis respectively; "scalability" represents multiple subjects; and Columns I, II, III, IV, V for "applications" are random motion synthesis without control signals, motion synthesis with control signals, motion denoising, motion completion and motion prediction. ✓ means good, × means poor and o means ok, namely between poor and good. -: Not implemented. Since PFNN[5] is designed to predict the pose for the next frame using phase values, not the probability distribution of the pose, it's not suitable for random motion synthesis. For fair comparisons, we only extend PFNN to controllable motion synthesis for multi-subjects by adding skeleton configuration as an additional input. We also extend LSTM networks to support multi-subject motion modeling (see Sec. 6 for details).

the personalized style implied in the motion and generate high-quality motions for the skeleton. Hence, the CCNet has the potential to be used as a pre-trained network in few-shot learning for motion modeling and synthesis.

We have built a large-scale motion database of 12 subjects with a variety of motion types and transitional clips between different types of motions. Complex motions, such as punching, kicking, and kicking while punching, are also included. The database has a total of 486,282 frames and will be made public with our code. Experimental results show that, with such a database and data augmentation, the CCNet can be efficiently trained, and it can generate high-quality motions fast (~65fps) in the inference. We show its advantages in the applications of motion processing and controllable motion synthesis for different subjects and styles. User studies verify that the quality of motions generated by our network is superior to the motions of state-of-the-art human motion modeling and synthesis methods.

2 Related Work

Human motion modeling and synthesis is a long-standing problem in the area of computer graphics. In the following, we focus our review on data-driven human motion modeling, as well as their applications in human motion synthesis and processing.

Motion Control and Synthesis. Data-driven motion synthesis is built successfully on the interpolation of motions in a database. For example, Rose et al. [9] classified the motion database into verbs and adverbs. Then human motions are interpolated by the constructed radial basis as well as low-order polynomials. However, interpolation-based methods can not adapt to the rich repertoire of human behaviors. Generative statistical models, which describe human movements by hidden parameters and the associated probability distributions, became the mainstream in the previous decades. Tanco et al. [10] learned a statistical model from the data set, and motion is then interpolated by giving the start and end frames, as well as a few keyframes with the learned statistical model. Other varieties of different statistical models, including Hidden Markov Models (HMMs) [11, 12], spatial-causal dynamic models [13, 14], and low-dimensional statistical models [15, 16] are developed one after the other for human pose analysis and synthesis. Furthermore, motion graphs [17, 18] and their various extensions [19, 20] are proposed to extend the statistical models for representing complex human motions. These directed graphs also provide benefits for the interactive editing and control for complex human motions. In [21], a generative motion graphs named MotionGraph++ is proposed to process motions at semantic and kinematic levels.

In this paper, we propose an end-to-end deep learning framework for human motion modeling and synthesis. Our deep-learning model is much more compact than motion graph++. Besides, our model has a much better generalization ability than motion graph++. Our experiments show that it can model not only a rich set of human actions and their transitions but also delicate motion variations across multiple subjects, a capability that has not been demonstrated in previous work.

Motion Style. Our method has superior performance for generating different motion styles associated with different people, even when they possess the same type of human motions. It is noted that *motion style* and *motion type* are

clearly differentiated in this paper. For example, a fat man and a thin man would have different walking styles for the same motion type, i.e., walking. The critical challenge is how to model the motion style. In the work of [12], the motion style is parameterized to learn a statistical model, and different types of motion can be synthesized from the learned model according to the input style parameters. Arikan et al. [19] proposed categorizing the human motions into different motion types, such as turning left and turning right, and then generating motion sequences according to the input motion types through a dynamic programming search algorithm. In the work of [26], the motion style for a single person has been proposed for addressing the problem of unlabeled heterogeneous motions. However, all the methods mentioned above only focus on the motion styles for a specific person. None of them can model the variations of human motion styles across different people. Similar to [27], our deep generative model can handle personalized style variations across multiple subjects. However, unlike [27], which can only model personalized style variations for a particular human motion such as walking or running, our generative model can scale up well to a rich repertoire of human motions as well as their transitions. Aberman et al. [28] handled the skeleton variations by representing skeletons as the static offsets in some arbitrary initial pose together with the dynamic motions in a tree graph structure. However, they focused on motion retargeting while we are interested in motion synthesis.

Deep Learning based Motion Synthesis. In recent years, deep learning has gained lots of attention in computer vision and computer graphics. Like many other tasks, such as image segmentation, classification, and object recognition, human motion synthesis has also benefited from the rapid progress of deep learning. It provides a remarkable tool for directly learning a compact, low-dimensional motion space from a dataset without any motion feature designations. By comparison, traditional successful generative statistical models for human motion synthesis heavily rely on the human-made ad-hoc motion features [16, 29, 20]. Holden et al. [30] proposed a convolutional auto-encoder to learn compact motion representation, termed as the motion manifolds, for human motion synthesis. Such motion representation can be utilized to fill in the missing data and perform the motion interpolation in the manifold space.

In [4], user-friendly high-level parameters for motion control, such as character motion trajectory and foot contact information, are investigated for synthesizing the human motions. Phase variable for cyclic motions is explicitly used as an input to control the weights in the network [5]. In contrast, the hidden state in LSTM can model the causal dependence of the motion implicitly. Thus motion synthesis with multi-objective control can be realized without the phase information [6]. Mixture-of-expert (MoE) architecture [31, 32, 33] are used to ease the burden of phase labeling for motions and improve the capacity of the networks for motion synthesis. Ling et al. [7] leveraged MoE as the decoder of motion VAEs to model the distribution of possible next poses. Starke et al. [34] added local motion phase feature to MoE to learn asynchronous movements of each bone and its interaction with external objects and environments. Reinforcement learning has been widely applied [35, 36, 37, 38, 39] to train physics-based motion controllers. Peng et al. [40] adopted a two-level hierarchical control policy with high-level environment information to make the character be aware of the surroundings. Won et al. [33] clustered the reference library of motions generated by the kinematic controller to construct experts and then combined these experts by deep reinforcement learning. The adversarial training strategy is adopted in [41, 36] to improve the quality of generated motions. Recently, mapping the features extracted from music [42] or language [43] to the motion space is utilized to generate character motions synchronizing with such multi-modal inputs.

Enormous neural networks are proposed to address long-term motion prediction problem, which include recurrent neural networks (RNNs) [2, 44, 45, 46], fully connected networks [47, 48], reinforcement learning [49, 50], graph networks [51, 52], and generative adversarial networks (GAN) [53]. To better model the randomness of human motions, Aliakbarian et al. [54] combined the root of variations with previous pose information to force the network to learn the motion variations. At the same time, Zhao et al. [55] exploited Bayesian Hierarchical Hidden semi-Markov Model (BH-HSMM) as generator and discriminators for adversarial learning. To solve the error accumulation problem for long-term motion prediction, practical strategies, including adding residual blocks and introducing sampling in training, are applied to improve RNN [3], and the auto-condition scheme is adopted in RNN in the work of [56]. QuaterNet [57] conducts extensive experiments to demonstrate that the quaternion representation is beneficial to improve the quality of synthesized motions.

Despite significant progress in deep-learning-based motion modeling and synthesis, constructing a generative model capable of accurately modeling motion data sets across different subjects remains challenging. The CCNet is more appealing to human motion modeling because the explicit causal convolution adopted in CCNet has a larger and more efficient receptive field than widely used networks such as RNNs or their variations. As shown in our comparisons (see Sec. 6), in the case of multiple subjects, the CCNet can capture personalized style variation and produce superior results than alternative deep learning models in terms of both motion synthesis quality and motion control accuracy, a capability that has not been demonstrated in previous work. Finally, as shown in Tab. 1, our model is more flexible and powerful for motion synthesis and processing. In contrast, traditional motion graph techniques [22, 23, 17, 21] are hard to scale up to handle large scale motion data, and the required memory footprint is usually large. For fair comparisons,

ERD-LSTM models [2, 3, 24, 6], DAE-LSTM models [25] and PFNN [5] are extended to model multi-subject motion data by taking skeleton configuration as an input (see Sec. 6 for details).

3 Overview

The overall framework of our system is illustrated in Fig. 1. Given the processed motion data (Sec.4), we train a CCNet to predict the PDF of the future pose conditioned on the poses of past frames and optional control signals, where the details of control signals are discussed in (sec. 4.2). The designed CCNet has three types of functional blocks, i.e., encoder, separate residual block, and decoder, and it outputs the mean and variance of the PDF (Sec. 5.1). A variety of motion synthesis applications, such as motion denoising, motion completion, and motion control, can be realized by this unified generative model with a single set of network parameters. We also test how the network generalizes to novel skeletons not in the training dataset (Sec. 6).

During training, we use Gaussian loss, foot contact loss, and smoothness loss to learn the network parameters (sec. 5.2). Noises are added to the sampled training motion data such that the trained network is robust to the accumulated error in the motion synthesis and can produce high-quality, non-freezing motions. The slight foot sliding in the generated motion is removed by an inverse kinematic (IK) algorithm according to the predicted foot contact label by the CCNet. To ease the interactive control, we also train the proposed network to output the direction and velocity control signal for the next frame.

4 Data Processing and Representation

We build a human motion database of 12 different subjects using the mocap technique. Three of the subjects are female, and the rest of them are male. The database includes 10 types of motions: walking, running, jumping with the left foot, jumping with the right foot, jumping with both feet, back walking, zombie-walking, kicking, punching and kicking while punching. All subjects are asked to perform the first 7 types of motions, and 5 of them are asked to perform the last 3 types of complex motions additionally. The motion recording speed is 120fps, and the recording time for each subject is within 2 hours. Thus, there are around 80,000 frames of motion data for each subject. During recording, we ask each subject to perform two types of motions in one motion sequence to facilitate the learning of transition between different motion types. Afterwards, We down-sample the recorded motion data to 60fps and obtain a total of 486,282 frames to be used as our training and validation datasets. The validation dataset is formed by randomly selecting one motion sequence of each subject. Moreover, all the motion sequences of subject 7 are removed from the training dataset and only present in the validation dataset, which is used to test how our network can handle the skeleton variation after training on multi-subject motion data. As a result, the validation dataset contains 41 motion sequences and a total of 88,649 frames. The rest motion data is used in the training dataset.

4.1 Motion representation

The character skeleton in the mocap data is modeled as an articulated figure with rigid links connected by ball-and-socket joints. The motion at each frame is recorded as the translation and rotation at the root joint and the relative rotations at other joints. However, such motion representation is a relatively local feature since most rotations at ball-and-socket joints are relative to their parent joint. Thus, we add 3D joint positions and the joints' angular and linear velocities into the representation to better model the global influence of joint rotations on rigid links' positions and orientations. Overall, the motion information at n_{th} frame is represented as $x_n = \{x_n^e, x_n^\omega, x_n^p, x_n^v, x_n^f\}$, where x_n^e denotes the vector of relative joint rotations represented using exponential coordinates [58], x_n^ω the vector of relative angular velocities of the joints, x_n^p the 3D joint positions, and x_n^v denotes the vector of joint linear velocities. The foot contact information at n_{th} frame is represented as a 2-dimensional binary vector x_n^f .

Before converting the mocap data into our representation, we first align each recorded motion clip by translating its first frame to the origin of the global coordinate system on the XOZ plane and setting the root's rotation around the global Y-axis to be zero. For the n_{th} frame in the clip, we first rotate the root orientation represented in the global coordinate system of frame $n - 1$ to a coordinate system whose Y-axis is $\{0, 1, 0\}$. We then represent the root position and orientation of n_{th} frame to the rotated coordinate system at frame $n - 1$. However, we still represent the y coordinate of the root joint in the global coordinate system to emphasize this quantity in network training. The rotations for non-root joints remain the same with the motion capture data. The linear and angular velocities are computed by subtracting the corresponding joint positions and rotations in exponential coordinates at frame n and $n - 1$ and representing the difference vectors in the rotated coordinate system of frame $n - 1$. The motion alignment makes our motion representation invariant to translation and facing orientation in the plane, which means that no matter where the

global root position and orientation of frame $n - 1$ are, the aligned motion representation remains the same as long as the relative motion is the same.

The foot contact information x_n^f is used to alleviate the foot sliding of the generated motions. It can be directly computed from the motion data. We first compute the distance between the current and the previous frame and their heights for the left and right toe joints. The height of the joint is just the y coordinate in our global coordinate system. If the distance and position y are less than the threshold $\delta_d = 5mm$ and $\delta_y = 80mm$ respectively, we set the foot contact label to be 1, otherwise 0.

4.2 Control Signal Representation

For the motion data at n_{th} frame, our system allows the user to input three types of control signals, which control the motions at future frames. The control signal is denoted by $c_n = \{c_n^d, c_n^t, c_n^s\}$, where c_n^d denotes the direction and velocity control, c_n^t the motion type control, and c_n^s the skeleton configuration signal used to differentiate subjects. The control signals used in training are extracted from the motion capture data.

Direction and velocity control. The control signal c_n^d is a 12-dimensional vector formed by sparsely sampling, in the causal domain, the points on the motion trajectory starting from n_{th} in a motion clip. Thus, this control signal also implicitly implies the velocity information. It is inspired by the trajectory used in [5], but we only use the future trajectory. Specifically, starting from the n_{th} frame in the clip, a motion sequence lasting for 1 second consisting of future frames is extracted, which is 60 frames in our 60fps motion capture setting. Second, we compute the 3D positions of root joints for all the extracted frames and then represent them in the n_{th} frame’s coordinate system. All the relative root positions are projected onto XOZ plane to obtain a future motion trajectory. Finally, the trajectory is uniformly down-sampled in the causal domain (every 10 frames) to 6 2D points to form the c_n^d . This procedure is repeated for all the frames in the motion database.

The direction control signal itself contains the velocity information because it is the heading trajectory in the next one second of future frames. Thus, it is not necessary to compute another velocity control signal for each frame. When the user needs to control the velocity of the motion, we allow the user to input the trajectory length for the future 1-second motion. It will be used to update the 6 points in c_n^d .

Motion type. Since our database consists of ten types of motions, the motion type control signal c_n^t is a 10-dimensional vector using one-hot coding. We manually label frames in the captured motion to obtain the motion type signal for training. However, it is difficult to give an exact type label for those transitional frames between two types of motions. Thus, when the transition happens, we treat the right-foot-touching-the-ground as the ending state of the first type of motion and the left-foot-leaving-the-ground as the starting state of the second type of motion. According to the frame index, we linearly interpolate the first type label vectors and the second type label vectors and assign the interpolation results as the motion type signal for the frames between the ending states and the starting states to the transitional frames.

Skeleton configuration. Since our database consists of different skeletons, the skeleton configuration is necessary to help the network to discern the skeleton variations across different persons. We transform the skeleton’s chain structure at T-pose into a control signal c_n^s that consists of the following components:

$$c_n^s = \{h_r, t_1^x, t_1^y, t_1^z, \dots, t_m^x, t_m^y, t_m^z\}, \quad (1)$$

where h_r is the height of the root joint, and the 3D positions of non-root joints, i.e., $\{t_1^x, t_1^y, t_1^z, \dots, t_m^x, t_m^y, t_m^z\}$, are set to be relative to the root. The number of joints m is set to be 27, which is the number of non-finger joints in our database. The 27 non-finger joints’ relative 3D positions and the root joint’s height form the 82 dimensions c_n^s . Note that the skeleton configuration is input to the network all the time, but other control signals are optional in the motion synthesis.

5 CCNet

In this section, we first describe the network structure of CCNet and then proceed to its training details.

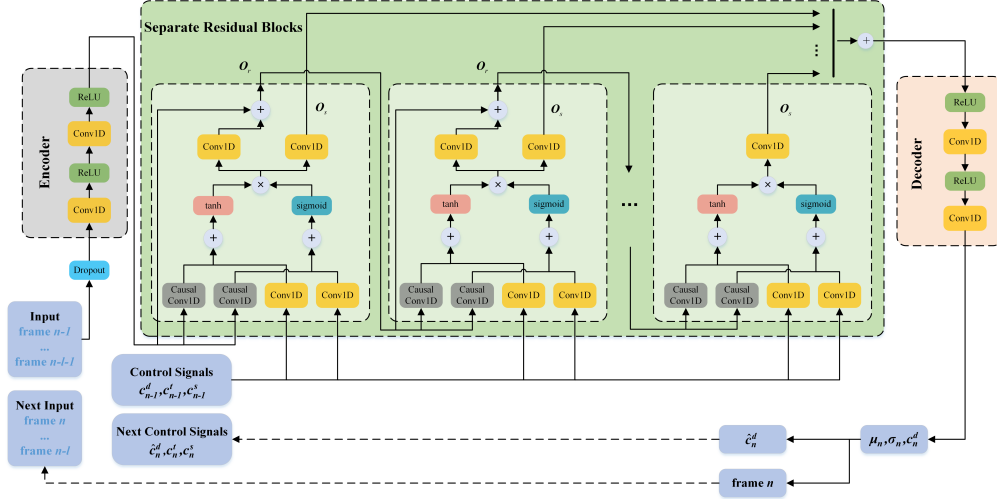


Figure 2: The network architecture of the CCNet. It consists of an encoder, separate residual blocks, and a decoder. The kernel size of Conv1D is set to 1, and the kernel size of CausalConv1D is set to 2 in all the blocks. Given the input frames, it outputs the Gaussian distribution of a future frame, direction control signal, and foot contact label.

5.1 The Network Structure

The network structure of our CCNet F is illustrated in Fig. 2 (detailed network parameters are reported in the supplementary material). It models the PDF of the predicted motion for n_{th} frame with the following formula:

$$p(x_n | X, c_{n-1}) = \psi(X, c_{n-1}) = \psi_D(\psi_R^0(\psi_E(X), c_{n-1}) + \sum_{i=1}^{19} \psi_R^i(\psi_R^{i-1, \dots, 0}(\psi_E(X)), c_{n-1})), \quad (2)$$

where $X = \{x_{n-1}, \dots, x_{n-l-1}\}$ and c_{n-1} are the motion data of past l frames and the control signals of $(n-1)_{th}$ frame. The dropout layer before the encoder, denoted by D , is used to resolve the possible over-fitting issue, and its drop probability is set to be 0.5.

The encoder ψ_E , the separate residual blocks (SRB) ψ_R^i , and the decoder ψ_D are the functional blocks in the network. There are a total of 20 SRBs in our network. The superscript $\{i-1, \dots, 0\}$ in Eq. 2 indicates that the SRBs in the network are recursively executed, and each i_{th} block takes the output of $(i-1)_{th}$ block and the control signals as its inputs. The first separate residual block ψ_R^0 takes the output from the encoder and the control signals as inputs. The output PDF $p(x_n)$ is set to be the Gaussian $\mathcal{N}(\hat{\mu}_n, \hat{\sigma}_n)$, where its mean $\hat{\mu}_n$ and standard deviation $\hat{\sigma}_n$ are the output of the decoder ψ_D . Since the decoder ψ_D might output a negative standard deviation value after convolution, we compute the final standard deviation values as $\hat{\sigma}_n = e^{\sigma_n}$, where σ_n is the direct output of the ψ_D .

Encoder. The motion representation X of past l frames are first input to an encoder ψ_E to map the data into features, and the encoder is of a simple "Conv1D-ReLU" structure where the size of 1D convolution kernel is 1 and use ReLU as the activation function. Note that the kernel of size 1 makes sure that the feature of the motion at each input frame is independent.

Separate residual blocks: The core component of the CCNet is the set of separate residual blocks ψ_R^i . It is similar to the residual blocks used in WaveNets [8], which use dilated causal convolution to guarantee the input motion data's ordering. The control signals are also inputted to the residual blocks through convolution layers with kernel size 1. The difference is that we use two separate dilated causal convolution layers and 1D convolution layers to compute separate features for the gated activation. This is designed to disentangle the information to increase the capacity of our network. Moreover, the features from the motion data and control signals are fused through summation. This enables us to switch on/off the control signals online during the training and inferring. The dilated Causal Convolution is implemented as in [8]. Specifically, zeros are padded before the feature of the $\psi_E(x_{n-l-1})$ so that the output of the convolution of a frame i only depends on the frames before it. The padding size can be easily computed as $(k-1) * d$, where k is the kernel size and d the dilation size. The kernel size of the causal convolution and dilation size in SRBs are set to be 2. As a result, the causal receptive field of the CCNet is 41 frames, which can be computed using the following formula:

$$F = (k-1) + \sum_{i=0}^{19} (k-1) * 2 \quad (3)$$

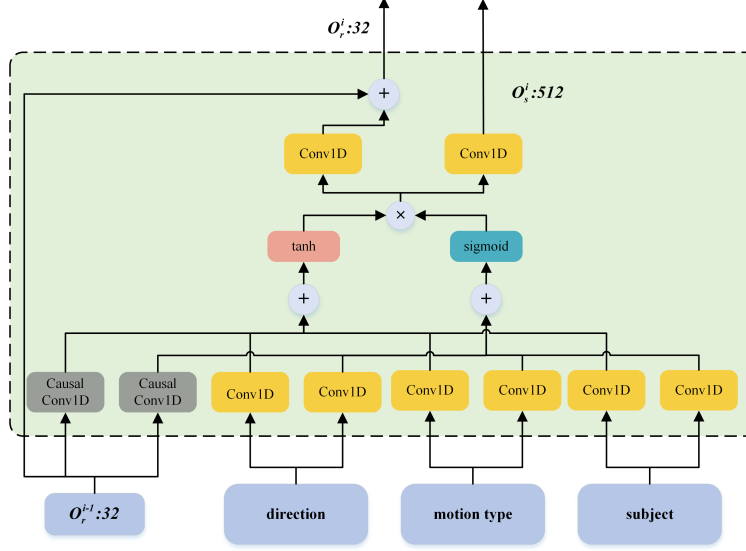


Figure 3: The detailed architecture of the separate residual block. The numbers besides O_r^{i-1} , O_r^i and O_s^i indicate the number of channels.

where k is 2, the kernel size of the dilated Causal Convolution used in our CCNet.

Fig. 3 shows the details on how the control signals are input to the separate residual blocks: each type of control signal is input to its own Conv1D layer, and the kernel size of Conv1D is 1. The input motion feature (channel number: 32) for SRB^i is the feature O_r^{i-1} output by SRB^{i-1} . The output feature O_s^i (dimensionality of the output features: 512) is sent to the decoder.

Decoder. The decoder ψ_D maps the summed features from the SRBs to the PDF of the predicted motion. It is of a simple "ReLU-Conv1D" structure, where the convolution kernel size is also set to be 1.

5.2 Training Loss

The training loss consists of four terms, a Gaussian loss L_G , a motion smoothness loss L_s , a foot contact label loss L_f and a direction control loss L_d . It can be formulated into:

$$L = L_G + \lambda_1 * L_s + \lambda_2 * L_f + \lambda_3 * L_d \quad (4)$$

where the weight λ_1 is set to be 10.0, λ_2 be 2.0 and λ_3 be 1.0 in all our experiments.

The first term L_G is the Gaussian loss. This term follows the Gaussian mixture loss in [2], while we only use one mode and set the covariance matrix to be diagonal to reduce the number of parameters. It can be written into:

$$L_G = -\ln(p(x_n | \hat{\mu}_n, \hat{\sigma}_n)), \quad (5)$$

where x_n is the motion representation extracted at n_{th} frame. Thus, this term enforces the network to output the values of mean $\hat{\mu}_n$ and standard deviation $\hat{\sigma}_n$ so that the captured motion data is of high probability. The binary foot contact label in x_n is handled in L_f and thus not included in this term. We add a constraint in our implementation to ensure the standard deviation $\hat{\sigma}_n$ is greater than $1e-4$ by a clipping operation, and we observe that the standard deviation output by the trained CCNet is usually between $1e-4$ and $1e-3$. Consequently, in motion synthesis, we can sample a motion according to the Gaussian distribution to enrich the variation of the synthesized motion. Note that the Gaussian function is used to maximize the probability of the motion representation vector of the ground-truth mocap data during training. Thus, the joint positions and linear velocities included in this term can help to model the correlations between the rotational degrees of freedom of different joints since such quantities are affected by all the parent joints on the kinematic chain connected to the joints.

The second term is the smoothness term to prevent the sudden change of the motion among neighboring frames, which is as follows:

$$L_s = \sum_{n=2}^N (\hat{\mu}_{n-2} + \hat{\mu}_n - 2\hat{\mu}_{n-1}). \quad (6)$$

The smoothness loss is only optimized for the mean of predicted Gaussian distributions since the motion generated by the network is usually close to the mean at each frame. This term is a soft constraint to prevent the sudden change of accelerations at joints and make the synthesized motion smoother.

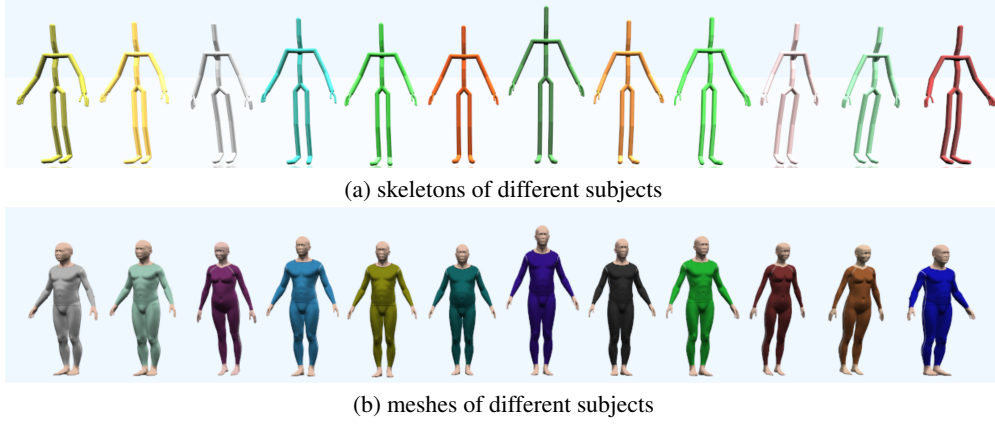


Figure 4: Skeletons and meshes in our database. The skeletons of subjects 0~11 are from left to right, and their heights are 160cm, 170cm, 168cm, 183cm, 172cm, 165cm, 195cm, 170cm, 178cm, 166cm, 155cm, 154cm, respectively. Subjects 2, 9, and 10 are female.

The third term is used to train the network to predict whether the foot is in contact with the supporting plane at n_{th} frame. Specifically, we adopt binary cross entropy(BCE) loss function to compute this term:

$$L_f = BCE(x_n^f, \hat{x}_n^f), \quad (7)$$

where x_n^f is the ground-truth foot contact label from the data, and \hat{x}_n^f is the network prediction. The foot contact label is used to trigger IK algorithms to remove the foot sliding in the synthesized motion.

The last term is used when the direction and velocity controls are switched on. It can be simply written as:

$$L_d = \|\hat{c}_n^d - c_n^d\|^2 + \|\hat{c}_n^v - c_n^v\|^2 \quad (8)$$

where c_n^d and c_n^v are the direction and velocity control signals computed from the motion data, and \hat{c}_n^d and \hat{c}_n^v are the predicted values. This term is useful in interactive motion control applications when control signals might be input by the user occasionally. In this case, the predicted control signal values will be fed into the network to continue the motion synthesis.

5.3 Training Details

We train our CCNet using the RMSProp optimizer [59]. The initial learning rate is 1e-4 and will be decayed by multiplying it by 0.5 every 500 epochs. The loss curve usually converges around 1000 epochs. The batch size is set to be 256, and each sample in the batch is a motion sequence of 240 consecutive frames. There are two steps to generate 240 samples in a batch: 1) randomly select a motion clip from the database and then the starting frame index in the clip. 2) Sample 240 frames in the clip repeatedly using a one frame interval, i.e., the starting frame index, F_{s+1} , of the next 240 frames sequence is equal to $F_s + 1$. For an input sequence, $X = \{x_0, x_1, \dots, x_{n-1}\}$, the CCNet can produce the output $Y = \{y_1, y_2, \dots, y_n\}$ due to the guaranteed causal ordering in all the dilated causal convolutional operations in CCNet. Thus, we can compute the training loss for all the output motions at different frames, which helps the CCNet learn to handle the input motions of different lengths.

Data augmentation. We add additional independent identically distributed Gaussian noises to each sampled motion representation vector of training motion data to train the network to handle accumulated errors in the motion synthesis. The mean and standard deviation of the noise is selected to be 0 and 0.03.

6 Experiments

We have implemented our algorithm using Pytorch 1.6 on a desktop PC with Intel(R) Xeon(R) Gold 5120 CPU, 128G RAM, and one Tesla V100 SXM2 32GB graphics card. The trained CCNet has 1.16M parameters, resulting in a model of size ~4.5M Bytes. The skeleton information is always input to the CCNet in both random and controllable motion synthesis since they are required to differentiate between subjects in the experiments. Although the network can generate high-quality motion, slight foot sliding might still occur. If not mentioned, the inverse kinematics algorithm is adopted to completely remove the foot sliding in the generated motion according to the predicted foot contact label. Besides, we denote the initial frames input to the CCNet to begin the motion generation as seed frames hereafter.

Baseline networks: We compare the CCNet to state-of-the-art motion synthesis networks that are listed below:

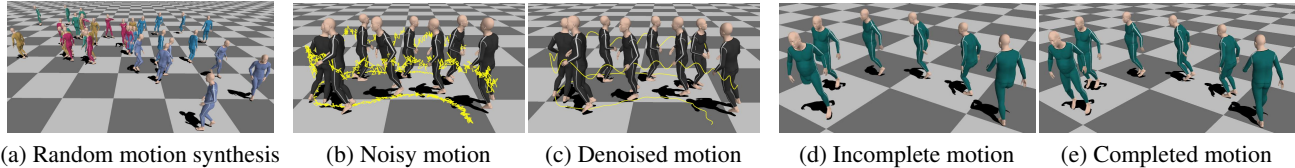


Figure 5: Random motion synthesis results. (a) Random motion generation result for subject 3 (the fourth skeleton shown in Fig. 4). Different colors of the clothing indicate the different random motions generated by the trained CCNet. (b) and (c) A motion denoising result for subject 7 (the eighth skeleton shown in Fig. 4). (d) and (e) A motion completion result for subject 5 (the sixth skeleton shown in Fig. 4).

- ERD-4LR: the encoder-recurrent-decoder network structure in [2]. We implement the network using 4 LSTM layers as in [6].
- DAE-LSTM: the network structure in [25] that uses a dropout autoencoder to filter the predicted poses output by an LSTM network.
- PFNN: the network structure in [5] that adopts a cyclic function to compute the neural network’s weights by taking the motion phase as an input.

To test these three network structures’ performance in multi-subject motion synthesis, we add parameters at their first layer to accept as input the skeleton configuration and the same set of control signals. For clarity, we refer to the modified networks for random motion synthesis as ERD-4LR-rand and DAE-LSTM-rand and the modified networks for controllable motion synthesis as ERD-4LR-cond and DAE-LSTM-cond. Since PFNN is mainly designed for controllable motion synthesis, not for a generative model, we only compare the CCNet with PFNN on controllable motion synthesis. We refer to the modified PFNN as PFNN-cond. Please refer to the supplementary_material.pdf in "other supplementary materials" for the detailed network parameters of the modified networks.

We separately train these five networks, namely ERD-4LR-rand, DAE-LSTM-rand, ERD-4LR-cond, DAE-LSTM-cond, and PFNN-cond, and our CCNet, on the multi-subject motion dataset. For all the networks, the initial learning rate is set to 1e-4, and it will be decayed by multiplying it by 0.5 every epoch. The batch size is 256, and each sample in the batch is a motion sequence of 240 consecutive frames. We train these networks for 2000 epochs. The rest training settings for baseline networks remain the same as reported in their papers. Please refer to [2], [6], [25] and [5] for the detailed settings. Finally, we choose the best-performed network snapshots that achieve the lowest validation loss as the final networks used in the comparisons. Specifically, the network snapshots are selected as follows: CCNet, ERD-4LR-rand, and ERD-4LR-cond: 1510th epoch, the PFNN-cond network: 1045th epoch, DAE-LSTM-rand: 1650th epoch, and DAE-LSTM-cond: 1120th epoch.

6.1 Random motion synthesis

Random motion generation: In this experiment, the skeleton configuration and seed frames are fed to the CCNet to generate high-quality motions. However, we do not input control signals, such as direction, velocity, and motion type, to the CCNet. Also, we use 120 seed frames to facilitate the comparisons since such length is chosen in ERD-4LR and DAE-LSTM [6, 25]. As illustrated in Fig. 5a, for the fourth skeleton shown in Fig. 4, five motion sequences are generated by sampling the pose at frame n using the predicted Gaussian distribution. The sampled pose is fed back to the network to generate future frames. The random motion generation can be used in motion prediction given a long motion sequence as an input, which is useful in on-line pose detection in computer vision or RGBD-based motion capture [60].

We also feed ERD-4LR-rand and DAE-LSTM-rand with the same 120 seed frames and the skeleton configuration to synthesize random motions for fair comparisons. As a result, we found that the CCNet, ERD-4LR-rand, and DAE-LSTM-rand can all synthesize long period motion sequences with more than 20,000 frames. The random motion generated by ERD-4LR-rand is also of good quality but a little bit less smooth than the motion generated by the CCNet. Comparisons conducted in the user study (Sec. 6.4) also show that the quality of the random motions generated by the CCNet is superior.

Motion denoising and completion: To test how the CCNet perform in motion denoising, we randomly select a motion sequence $X = \{x_0, x_1, \dots, x_k\}$ of a subject and then add independent identically distributed Gaussian noise (mean 0, standard deviation 0.01~0.1) to the motion data \hat{X} . The network takes \hat{X} as an input and outputs the denoised motion Y . However, the denoised pose is not fed back into the network, which is different from the random motion generation. For those frames with indices less than the casual receptive length, 41 frames in our network, they are denoised according to all the frames before them since the CCNet is trained to handle motions of different lengths. Fig. 5b and 5c illustrate

Noise STD	Denoising Errors (mean±std)		
	ERD-4LR-rand	DAE-LSTM-rand	CCNet
0.03	0.768±0.357	0.687±0.384	0.528±0.126
0.05	0.768±0.357	0.687±0.384	0.539±0.125
0.1	0.77±0.361	0.687±0.384	0.584±0.117

Table 2: Motion denoising comparison. STD: standard deviation. IK is disabled in this experiment. The errors of the motions denoised by the CCNet are less than the errors of the motions denoised by ERD-4LR-rand and DAE-LSTM-rand.

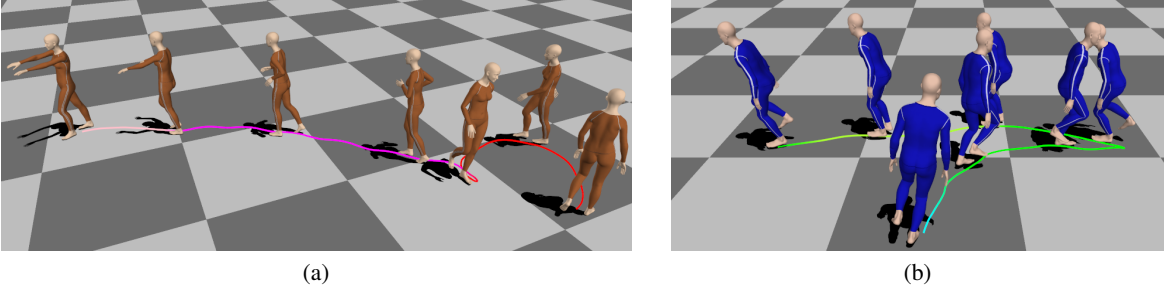


Figure 6: Trajectory-following results of two subjects. (a) A synthesized motion transiting from walking to running then to zombie walking for subject 10 (the eleventh skeleton shown in Fig. 4). (b) A synthesized motion transiting from jumping with the right foot to jumping with the left foot then to jumping with both feet for subject 11 (the twelfth skeleton shown in Fig. 4). We use different colors to represent different motion types at the different part of trajectories as follows: red-> walking, magenta->running, green->jumping with the left foot, cyan->jumping with the right foot, green-yellow->jumping with both feet, blue->back walking, pink->zombie walking, orange->kicking, purple->punching, and brown->kicking while punching.

a denoising result. The standard deviation of the noise for this experiment is set to 0.08. Before denoising, the right hand and right toe’s trajectories are very jerky, and the foot is underneath the ground at some frames. It can be seen that these artifacts are significantly reduced in the denoised motion. To compare the CCNet to baseline networks in the quality of denoised motions, we add Gaussian noise to the test data with standard deviations 0.03, 0.05, and 0.1, respectively, and then use CCNet, DAE-LSTM-rand, and ERD-4LR-rand to denoise the noisy motion data. The error between the ground truth motion and the denoising result is computed as the Euclidean distance between their motion representation vectors as described in Sec. 4. As shown in Tab. 2, the error of the denoised motion generated by the CCNet is less than the motions denoised by DAE-LSTM-rand and ERD-4LR-rand.

The procedure of motion completion is similar to motion denoising. In the experimental results illustrated in Fig. 5d and 5e, we first select a 700-frame motion sequence containing walking and jumping with both feet, and then set the rotations of joints of the right legs of 30% frames to 0. The CCNet takes the incomplete motion as the inputs and outputs a completed naturally looking motion.

6.2 Controllable motion synthesis

Motion control using user-specified trajectories: Synthesizing different types of motions along a specified trajectory is a desirable function in motion planning. We allow users to specify a motion trajectory J on the XOZ plane with additional velocity and motion type information and then map the trajectory information into the control signals c_n^d and c_n^t supported in our system. Specifically, the trajectory J is represented as $J = \{\{J_i, t_i, v_i\}, i = 1, \dots, k\}$, where J_i is the i_{th} part of the whole trajectory represented as an ordered densely sampled 2D points, the motion type information t_i , and a scalar velocity value v_i are also associated to the J_i . For two adjacent parts of the trajectory with different motion types, we set up 20 transitional frames with interpolated motion type control signal (see Sec. 4 for the details of motion type interpolation).

Suppose we already synthesize frame n , and its root position projected on the XOZ plane, denoted by t_n^p , might deviate from the input trajectory. We first find the closest point t^J on the J , and then extract the part of trajectory \hat{J}^E lasting for one second starting from t^J using the specified velocities. We then linearly interpolate between \hat{J}^E and the line connecting t_n^p and the endpoints of the expected trajectory \hat{J}^E to obtain a blended trajectory \hat{J}^b . The blending weight for the \hat{J}^E starts with 0 and increases towards 1 according to the time parameter. Afterward, 6 2D points are uniformly

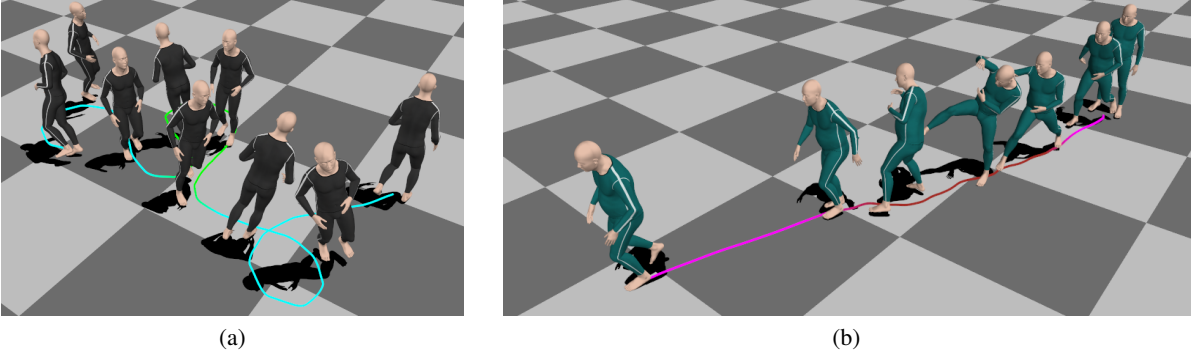


Figure 7: Our CCNet can synthesize (a) motions heading along a complex trajectory and (b) Complex motions for subject 5 (the eighth skeleton shown in Fig. 4).

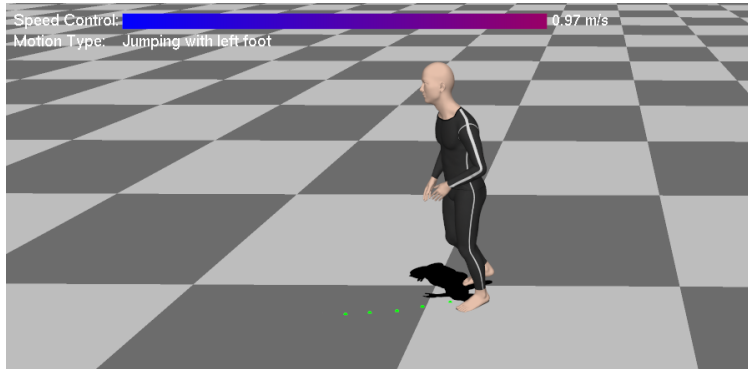


Figure 8: The user interface for interactive control. The green dots on the ground represent the direction control signal. IK is disabled.

sampled in the causal domain from \hat{J}^b to be input as the c_n^d . All the sampled points are represented into the root orientation at frame n as described in Sec. 4.

As shown in Fig. 6, our system can synthesize motions following two user-specified trajectories. Different trajectory colors indicate different types of motion. Fig. 7a illustrates that the synthesized motions can well follow a trajectory with large curvatures and frequent change of motion types. In Fig. 7b, we show that the CCNet can generate complex motions, such as kicking and punching motions present in our training dataset, when the user specifies these two motion types along a trajectory.

Interactive control: The CCNet can be easily integrated into interactive applications, and we demonstrate this capability by developing a demo that allows the user to control the direction, velocity, and motion type through a keyboard. Direction and velocity signals are used to generate future motion trajectory c_n^d online similar to PFNN [5]. The PyTorch implementation is exported to C++ through the LibTorch API to ease the implementation of this demo.

Specifically, to control the motion type, the user can use the number keys from 1 to 5 to select among 5 motion types: walking, running, jumping with the left foot, jumping with the right foot, and jumping with both feet. Once a key (for instance, 2) is pressed down, we update the motion type label by interpolating the new type label with the previous one in 20 frames, which means the character can transition from the previous motion type to the new one more smoothly. The user can also control the velocity by pressing up and down keys and heading direction of the character by pressing the left and right keys. Once the left key is pressed, the trajectory will be turned left. It is achieved by first computing a small offset vector $o_n = [1, 0] * h * 0.015$, where h is the root’s height. This offset will be added to the c_n^d by $o_n * w_i$, where $w_i = i/5, i = 0.5$. Thus, the offset will be added to the 6 points in the predicted control signal \hat{c}_n^d through the corresponding w_i . The distance between the 2D points in the updated \hat{c}_n^d is then adjusted according to the user-specified velocity v_u . Since the \hat{c}_n^d represents the future motion trajectory within one second, we can adjust the distance between its 2D points by multiplying it by the ratio between the current scalar velocity of the character v_{cur} (computed by the length of the 2D points in c_n^d) and v_u , which is v_u/v_{cur} . The velocity is changed from the current velocity to the user-specified velocity with 20 frames interval. Fig. 8 illustrates the user interface used in interactive control.

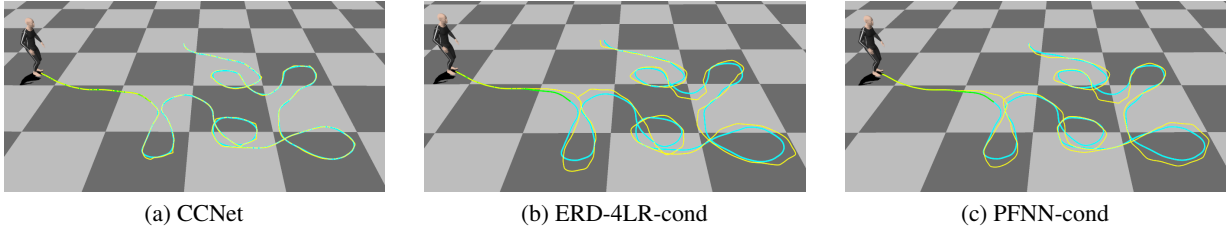


Figure 9: Comparisons against ERD-4LR-cond and PFNN-cond. The character starts by jumping with the left foot, then changes to jumping with the right foot till the end. The total errors between the synthesized trajectories (the yellow lines) and the input trajectories (the green lines) of ERD-4LR-cond, PFNN-cond and the CCNet are 177.143cm, 156.604cm and 27.043cm, respectively. IK is disabled in this experiment.

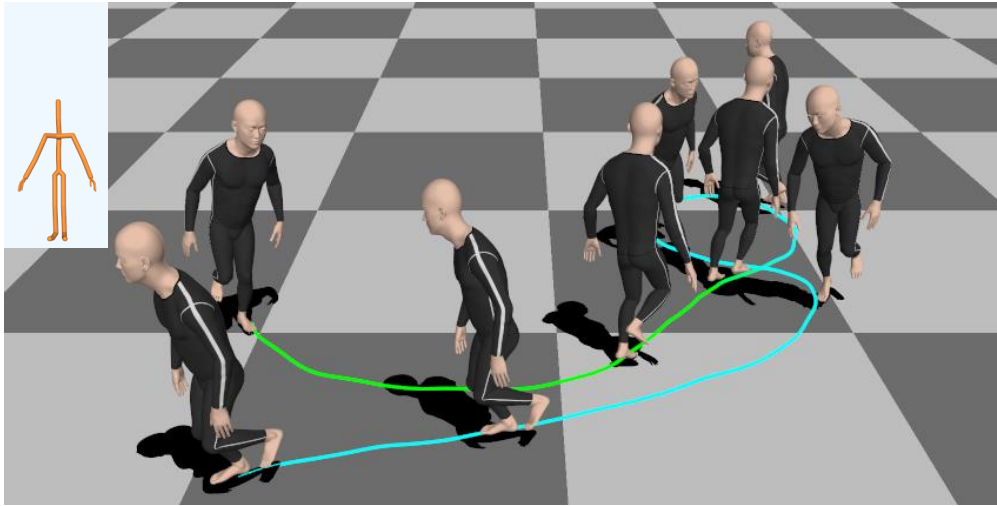


Figure 10: Trajectory-following results generated by the CCNet for an unseen skeleton subject 7_b. The skeleton of subject 7_b is generated by scaling the lower body of subject 7’s skeleton by 0.8. Please see the accompanying video from 2m 44s to 3m 3s for the demo.

Comparisons: We first compare the CCNet with baseline models on how accurate the generated motion is with respect to the user-specified trajectory. Thus, we leverage the average distance between the user-specified trajectory and the root trajectory on the XOZ plane as the criterion. In this accuracy experiment, with six different trajectories manually specified by users, we extract the direction control signals and randomly assign motion type information to trajectory segments. Afterward, we synthesize motions using the first 120 frames of the 33 locomotion sequences in the validation dataset as the seed frames for each specified trajectory and get a total of 198 controllable motion synthesis results. The trajectory distance is computed by summing the closest distance between a projected root position and a target trajectory at each frame. The mean and standard deviation of the averaged trajectory distance is as follows: 27.878 ± 8.516 for the CCNet, 158.67 ± 30.94 for PFNN-cond, and 171.973 ± 31.862 for ERD-4LR-cond. Fig. 9 shows an example. The result of the CCNet is more accurate than the baseline models. We will show the six trajectories in the supplementary material.

We also compare the motion quality in the case of controllable motion synthesis through a user study (see Sec. 6.4 for details). The user study results also verify that the CCNet can generate controllable motions of better quality in the setting of multi-subjects.

6.3 Generalization to Unseen Skeletons

After training with multi-subject motion data, the CCNet can generate motions for skeletons not in the training dataset. As illustrated in Fig. 4, 5b, 5c, and 7a, we have applied the trained CCNet to automatically generate denoised and controllable motions for the skeleton of subject 7 not in the training dataset. We also test the generalization ability of the CCNet by applying it to a particularly designed skeleton generated by scaling the skeleton of subject 7. Fig. 10 illustrates that the CCNet can generalize well to the new skeleton. Since there is no mocap data for it, we utilize motion

	Models	Relative Pose Difference (mean±std)
CCNet on entire dataset	no fine-tuning	0.083±0.0925
	fine-tuning with walking data	0.0536±0.0365
	fin-tuning with walking and running data	0.0483±0.0544
CCNet on dataset1	no fine-tuning	0.0861±0.155
	fine-tuning with walking data	0.0543±0.0646
	fin-tuning with walking and running data	0.0525±0.0594
CCNet on dataset2	no fine-tuning	0.0914±0.108
	fine-tuning with walking data	0.0598±0.077
	fine-tuning with walking and running data	0.059±0.0713

Table 3: The influence of the fine-tuning of CCNet with partial motion data of an unseen skeleton subject 7. Dataset1 contains motions of subjects 1, 3, 4, 8 and dataset2 contains motions of subjects 0, 5, 6, 11. Fine-tuning with walking and running mocap data of subject 7 with our entire training dataset (third row) achieves the lowest relative pose difference. IK is disabled in this experiment.

VS	RAND		CONTR		
	ERD-4LR-rand (mean: 3.065, std: 1.39)	DAE-LSTM-rand (mean: 1.75, std: 0.968)	ERD-4LR-cond (mean: 2.75, std: 1.199)	DAE-LSTM-cond (mean: 0, std: 0)	PFNN-cond (mean: 2.375, std: 0.992)
CCNet (RAND: mean: 6.25, std: 1.09 CONTR: mean: 6.625 std: 1.615)	P-value: 9.1671e-8 t-value: -6.9878	P-value: 6.1188e-13 t-value: -11.9588	P-value: 2.7365e-8 t-value: -7.4383	P-value: 1.7796e-16 t-value: -16.3353	P-value: 1.0127e-9 t-value: -8.7165

Table 4: T-test of user-study in the cases of random and controllable motion synthesis (confidence interval=0.95). VS: performing t-test between the results of the CCNet and all the results of baseline models in the second row. RAND: random motion synthesis. CONTR: controllable motion synthesis. Mean: the average number of generated sequences selected by all the participants after comparing to mocap sequences in the same group. Std: the standard deviation of the number being selected.

retargetting [61] algorithm to generate 120 seed frames for the new skeleton. Besides, we use ERD-4LR-cond and PFNN-cond to generate motions for the skeleton. The results show that motions generated by both of them contain big sudden changes between seed frames and generated frames, which is inferior to the motion generated by the CCNet.

Moreover, the CCNet can be used as a pre-trained network in few-shot learning for motion modeling and synthesis. Given a few motion data of a novel skeleton, it can learn to capture the personalized style implied in the motion for the skeleton. Tab.3 shows that, after finetuning the network on the walking and running motion of subject 7, the relative pose difference, rel_p , for all mocap data of this subject in the validation dataset can be significantly reduced. We compute relative pose difference as $rel_p = \frac{1}{N} \sum_{n=0}^N (\|\hat{x}_n - x_n\|_2 / \|x_n\|_2)$, where N is the number of frames, and \hat{x}_n and x_n are the motion representation vectors of motions generated by the finetuned CCNet and the corresponding mocap data. The ability of generalization to new skeletons is crucial since it can save efforts to capture a large number of high-quality mocap data for a new skeleton in the motion synthesis applications.

To evaluate how the number of subjects in the dataset influences the generalization ability of the CCNet, we intentionally put the motions of subjects 1, 3, 4 and 8 into dataset1 and the rest motions of subjects 0, 5, 6 and 11 to dataset2. Tab. 3 lists the statistics of rel_p of the motion generated by the CCNet finetuned on dataset1 (CCNet on dataset1) and dataset2 (CCNet on dataset2). Since the heights of subjects 1, 3, 4 and 8 are closer to subject 7’s height, the rel_p of CCNet on dataset1 is less than that of dataset2, but still larger than that of CCNet trained with all mocap data in the training dataset. Thus, to improve the generalization ability of the CCNet to new skeletons, it is better to construct a database with more subjects for the network to learn how to handle skeleton variations.

6.4 User Study

We perform a t-test to verify the hypothesis that the CCNet can generate motions of better quality than baseline models. To this end, we design the user study as follows. First, we present 16 participants with all groups of motion sequences: three groups for random motion synthesis and four groups for controllable motion synthesis. Each group contains 16 pairs of motion sequences. One is the mocap sequence, and the other is generated by the CCNet or one of the baseline models (Please refer to the supplementary_material.pdf in "other supplementary materials" for the details of motion generation in the user study). Second, we ask the participants to select which sequence in a pair is of better motion quality. If the chosen number of CCNet-generated motion sequences is larger than the chosen number for other baseline models with statistical significance, we deem that our hypothesis is verified. The participants include six females and ten males, and all of them have experience with 3D animation or games. Before the user study, we present a few mocap sequences to the participants as examples of goog-quality motions. Besides, if there are sudden changes or

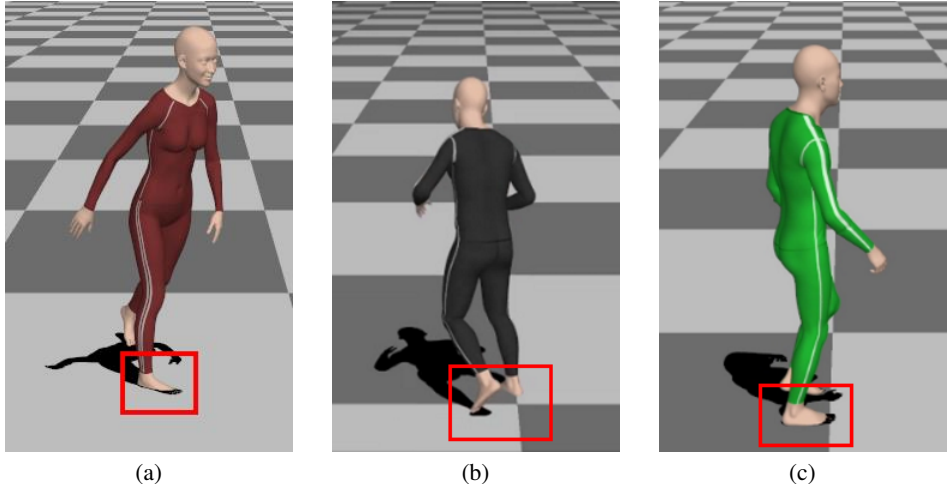


Figure 11: Foot-ground penetrations in the motions generated by DAE-LSTM-rand, ERD-4LR-cond and PFNN-cond. (a) The 611th frame generated by DAE-LSTM-rand for subject 9 in random motion synthesis. (b) The 450th frame generated by ERD-4LR-cond for subject 7 in controllable motion synthesis. (c) The 666th frame generated by PFNN-cond for subject 8 in controllable motion synthesis. DAE-LSTM-rand, ERD-4LR-cond and PFNN-cond can not effectively differentiate styles of different skeletons and lead to the foot-ground penetrations, as indicated by red rectangles. Furthermore, the motions generated by the CCNet is smoother.

Groups	numbers for CCNet (mean±std)
ERD-4LR-rand vs. CCNet	10.94±1.56
DAE-LSTM-rand vs. CCNet	12.31±2.34
ERD-4LR-cond vs. CCNet	11.63±2.87
DAE-LSTM-cond vs. CCNet	16±0.0
PFNN-cond vs. CCNet	11.445±1.87

Table 5: The average selected number for CCNet-generated motion sequences. Baseline-X vs. CCNet: a group of 16 pairs of motion sequences generated by a baseline model and the CCNet. Mean±std: mean and variance of the number of CCNet-generated motion sequences selected by all the participants.

foot penetrations into the ground plane, the sequence should be regarded as the worse one. At last, we get 15 valid questionnaires for random motion synthesis and 16 for controllable motion synthesis.

The t-test results are shown in Tab. 4. The P-values of the CCNet vs. other baseline models are all less than the selected threshold (0.05). Therefore, the motions generated by the CCNet are significantly different from the motions generated by baseline models. According to the average number of motion sequences selected by the participants (mean in Tab. 4), the average number of selected motion sequences of CCNet is larger than that of other baseline models. It verifies that the CCNet can generate better motions than state-of-the-art baseline models in different scenarios (The ANOVA test result in the supplementary material also verifies the statistical significance of the user study). Furthermore, we prepare another 5-group data that contain pairs of motion sequences generated by the CCNet and each baseline model. As listed in Tab. 5, the number of CCNet-generated motion sequences selected by participants is still larger than that of the sequences generated by baseline models. Fig. 11 shows examples of generated motion sequences used in this study. Motion jittering and penetrations into the ground plane frequently happen for motion sequences generated using ERD-4LR-cond, ERD-4LR-cond, and PFNN-cond, which indicates that these models can't handle the skeleton variations as well as the CCNet. In addition, we observe that DAE-LSTM-cond fails to generate long-period, controllable motion.

6.5 Evaluation of Network hyper-Parameters and Training Settings

In this section, we report the experiments conducted to figure out the hyper-parameters and training settings selected for the CCNet, including causal receptive length (CRL), numbers of consecutive frames of each sample in a batch (NCF), the length of seed frames, and the choice of smoothness loss term. We conduct all the experiments on the same training and validation datasets to verify our choices. Precisely, the chosen hyper-parameters for our CCNet in the random and controllable motion synthesis experiments above are as follows: CRL=41 and NCF=240. They are selected to minimize the loss in Eq. 2 computed on mocap data in the validation set. For better visualization, the loss curves are plotted

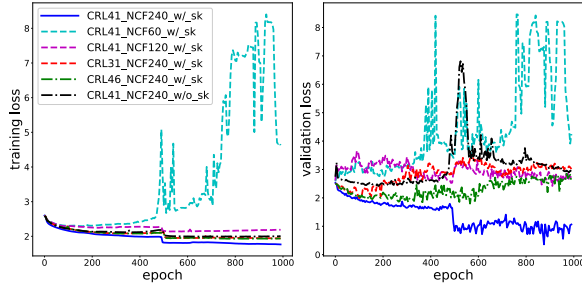


Figure 12: Loss curves obtained using different hyper-parameters of the CCNet. Left: Training. Right: Validation. We modify each hyper-parameter, including CRL, NCF and with/without skeleton configuration (w/_sk or w/o_sk), and compute the losses on the training and validation datasets respectively.

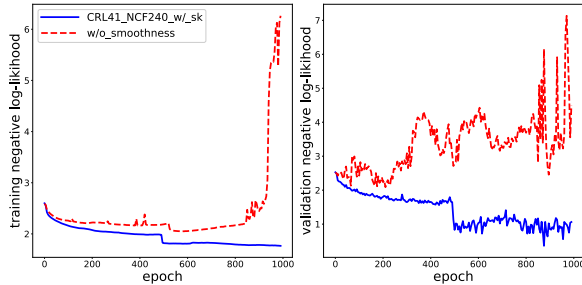


Figure 13: Ablation study of smoothness loss term. We remove the smoothness loss term and evaluate the corresponding re-trained model. Left: Training. Right: Validation.

using the formula $\log_{10}(loss + 320)$, where the loss is computed using Eq. 2. A bias 320 is added to make $loss + 320$ positive since the loss value is usually around -300 .

Causal receptive length: We conduct experiments to choose the causal receptive length among three choices: 31 (with dilations of SRBs being repeatedly 1, 2), 41 (with dilations of SRBs being repeatedly 2), and 46 (with dilations of SRBs being repeatedly 1, 2, 4), numbers of SRBs are fixed at 20 and we keep all the other settings the same as described in Section. 5.1. When the causal receptive length is 31 and 46, the network converges to higher loss after training on the training dataset, as shown by the red dashed lines and green dash-dot lines in Fig. 12. We choose CRL as 41 that can lead to the lowest loss in this experiment.

NCF in a batch: We also test the NCF of each sample in a batch, which is set to be 60, 120, and 240, respectively. These numbers correspond to 1 second, 2 seconds, and 4 seconds long sequences. This can be easily achieved by changing the frame numbers in a batch and keep the other parameters the same. For the comparison’s convenience, we keep the numbers of consecutive frames of each sample in a batch fixed as 240 when computing the loss on the validation dataset. The cyan dashed lines in Fig. 12 illustrate that both training and validation loss exploded before converging when NCF is 60. The magenta dashed lines in Fig. 12 show that the network converges to a higher loss in the case of NCF=120, comparing to NCF=240. We hypothesize that 60 and 120 consecutive frames result in inadequate training data in a batch and too noisy gradient when training the network. Thus, we set NCF to 240 frames in training.

The importance of the skeleton configuration and the smoothness loss term: It is implemented by disconnecting the 1D convolution module for the skeleton configurations signal to the network and check whether the loss on the validation set increases significantly. The black dash-dot lines in Fig. 12 indicate that the network without skeleton configuration converges to a much higher loss when training on our multi-subject training dataset. However, the loss explodes at around 700 epochs on the validation dataset. Thus, the skeleton configuration plays an important role in the network to disambiguate different subjects’ motions. To verify the importance of smoothness loss term to the CCNet, we train the network by removing it from the loss terms. Fig. 13 indicates that the loss curves on both training and validation datasets explode before converging without smoothness term, which means the smoothness term is essential for the network to prevent the generated motions from big sudden changes and converge to a better result.

Seed frame length: The influence of seed frame length on the quality of generated motions is measured by computing the relative pose differences between generated motion and corresponding mocap data. Specifically, we extract seed frames from mocap data in the validation dataset and then let the networks predict a frame to be compared with the corresponding mocap frame in the case of controllable motion synthesis. Tab. 6 shows the computed relative pose

seed frame numbers	Relative Pose Difference (mean/std)		
	ERD-4LR-cond	DAE-LSTM-cond	CCNet
1	0.214±0.302	0.56±0.572	0.13±0.179
5	0.18±0.145	0.325±0.508	0.091±0.128
10	0.14±0.159	0.303±0.49	0.084±0.136
30	0.145±0.179	0.182±0.27	0.074±0.128
60	0.12±0.138	0.178±0.253	0.074±0.124
120	0.126±0.16	0.115±0.144	0.074±0.125

Table 6: Ablation study on the length of seed frames in the case of controllable motion synthesis. We synthesize motion sequences using different lengths of seed frames to check their influences on the generated motions. IK is disabled in this ablation study.

difference rel_p (see its definition in Sec. 6.3) for different seed frame length, such as 1, 5, 10, 30, 60 and 120. The lower difference value indicates that the generated motion is more similar to mocap data and thus of better quality. It can be seen that the CCNet is robust to the variation of the length of seed frames comparing to ERD-4LR-cond and DAE-LSTM-cond, and it doesn't need too long seed frames to synthesize high-quality motions. However, we observe that there are more obvious jitters between the seed frames and the generated frames in the cases of 1 and 5 seed frame lengths. We hypothesize that, for such short length seed frames, the CCNet can't get enough information to generate smooth motions.

7 Conclusion

We have designed a deep generative motion model, i.e., CCNet, based on causal convolution proposed in WaveNet [8] to synthesize high-quality motions for multiple subjects. The trained CCNet can also synthesize several types of complex motions, such as punching, kicking, and kicking while punching, included in our database. The CCNet can be applied to various applications, such as random motion generation, motion denoising, motion completion, and controllable motion synthesis. Moreover, the CCNet can generate motions for novel skeletons. Given sample motions of a novel skeleton, the pre-trained CCNet can be fine-tuned to capture the skeleton's motion style.

Limitation and future work: Currently, the CCNet trained on our database can not handle arbitrary skeleton variation. For instance, if we scale the lower body of a skeleton in our database with a ratio less than 0.6, the CCNet without fine-tuning will generate motions with severe foot-ground penetration for the scaled skeleton. We hypothesize that it is because that 11 different skeletons in our training set might not be enough for the network to learn how to handle the large space of skeleton variation. Therefore, we plan to increase the number of subjects in the database to investigate the capacity of the CCNet. In addition, we also plan to increase the number and types of complex motions in the database to improve the quality of complex motion generation. Another issue with our CCNet is the number of seed frames required to initialize the motion synthesis. When seed frame length is set to between 1 and 5, jitters will occur in the generated motion, which might limit the application of the CCNet to model swift motions. We are also interested in investigating to take more temporal information as input, for instance, phase-like information in PFNN or joint accelerations, to mitigate this issue.

References

- [1] Graham W Taylor and Geoffrey E Hinton. Factored conditional restricted boltzmann machines for modeling motion style. In *Proceedings of the 26th annual international conference on machine learning*, pages 1025–1032. ACM, 2009.
- [2] Katerina Fragkiadaki, Sergey Levine, Panna Felsen, and Jitendra Malik. Recurrent network models for human dynamics. In *Proceedings of the IEEE International Conference on Computer Vision*, pages 4346–4354, 2015.
- [3] J A Martinez, Michael J Black, and Javier Romero. On human motion prediction using recurrent neural networks. pages 4674–4683, 2017.
- [4] Daniel Holden, Jun Saito, and Taku Komura. A deep learning framework for character motion synthesis and editing. *ACM Transactions on Graphics (TOG)*, 35(4):138, 2016.
- [5] Daniel Holden, Taku Komura, and Jun Saito. Phase-functioned neural networks for character control. *ACM Trans. Graph.*, 36(4), July 2017.
- [6] Kyungho Lee, Seyoung Lee, and Jehee Lee. Interactive character animation by learning multi-objective control. *ACM Trans. Graph.*, 37(6), December 2018.

- [7] Hung Yu Ling, Fabio Zinno, George Cheng, and Michiel van de Panne. Character controllers using motion vaes. 39(4), 2020.
- [8] Aaron van den Oord, Sander Dieleman, Heiga Zen, Karen Simonyan, Oriol Vinyals, Alex Graves, Nal Kalchbrenner, Andrew Senior, and Koray Kavukcuoglu. Wavenet: A generative model for raw audio, 2016.
- [9] Charles Rose, Michael F Cohen, and Bobby Bodenheimer. Verbs and adverbs: Multidimensional motion interpolation. *IEEE Computer Graphics and Applications*, 18(5):32–40, 1998.
- [10] Luis Molina Tanco and Adrian Hilton. Realistic synthesis of novel human movements from a database of motion capture examples. In *Proceedings Workshop on Human Motion*, pages 137–142. IEEE, 2000.
- [11] Richard Bowden. Learning statistical models of human motion. In *IEEE Workshop on Human Modeling, Analysis and Synthesis, CVPR*, volume 2000, 2000.
- [12] Matthew Brand and Aaron Hertzmann. Style machines. In *Proceedings of the 27th annual conference on Computer graphics and interactive techniques*, pages 183–192. ACM Press/Addison-Wesley Publishing Co., 2000.
- [13] Jinxiang Chai and Jessica K Hodgins. Constraint-based motion optimization using a statistical dynamic model. In *ACM Transactions on Graphics (TOG)*, volume 26, page 8. ACM, 2007.
- [14] Xiaolin Wei, Jianyuan Min, and Jinxiang Chai. Physically valid statistical models for human motion generation. *ACM Transactions on Graphics (TOG)*, 30(3):19, 2011.
- [15] Keith Grochow, Steven L Martin, Aaron Hertzmann, and Zoran Popović. Style-based inverse kinematics. In *ACM transactions on graphics (TOG)*, volume 23, pages 522–531. ACM, 2004.
- [16] Jinxiang Chai and Jessica K Hodgins. Performance animation from low-dimensional control signals. *ACM Transactions on Graphics (ToG)*, 24(3):686–696, 2005.
- [17] Jehee Lee, Jinxiang Chai, Paul SA Reitsma, Jessica K Hodgins, and Nancy S Pollard. Interactive control of avatars animated with human motion data. In *ACM Transactions on Graphics (ToG)*, volume 21, pages 491–500. ACM, 2002.
- [18] Rachel Heck and Michael Gleicher. Parametric motion graphs. In *Proceedings of the 2007 symposium on Interactive 3D graphics and games*, pages 129–136. ACM, 2007.
- [19] Okan Arikan, David A Forsyth, and James F O’Brien. Motion synthesis from annotations. In *ACM Transactions on Graphics (TOG)*, volume 22, pages 402–408. ACM, 2003.
- [20] Yongjoon Lee, Kevin Wampler, Gilbert Bernstein, Jovan Popović, and Zoran Popović. Motion fields for interactive character locomotion. In *ACM Transactions on Graphics (TOG)*, volume 29, page 138. ACM, 2010.
- [21] Jianyuan Min and Jinxiang Chai. Motion graphs++: a compact generative model for semantic motion analysis and synthesis. *ACM Transactions on Graphics (TOG)*, 31(6):153, 2012.
- [22] Okan Arikan and David A Forsyth. Interactive motion generation from examples. In *ACM Transactions on Graphics (TOG)*, volume 21, pages 483–490. ACM, 2002.
- [23] Lucas Kovar, Michael Gleicher, and Frédéric Pighin. Motion graphs. In *ACM SIGGRAPH 2008 classes*, page 51. ACM, 2008.
- [24] Yi Zhou, Zimo Li, Shuangjiu Xiao, Chong He, Zeng Huang, and Hao Li. Auto-conditioned recurrent networks for extended complex human motion synthesis. 2018.
- [25] Partha Ghosh, Jie Song, Emre Aksan, and Otmar Hilliges. Learning human motion models for long-term predictions. In *2017 International Conference on 3D Vision (3DV)*, pages 458–466. IEEE, 2017.
- [26] Shihong Xia, Congyi Wang, Jinxiang Chai, and Jessica Hodgins. Realtime style transfer for unlabeled heterogeneous human motion. *ACM Transactions on Graphics (TOG)*, 34(4):119, 2015.
- [27] Jianyuan Min, Huajun Liu, and Jinxiang Chai. Synthesis and editing of personalized stylistic human motion. In *Proceedings of the 2010 ACM SIGGRAPH symposium on Interactive 3D Graphics and Games*, pages 39–46, 2010.
- [28] Kfir Aberman, Peizhuo Li, Dani Lischinski, Olga Sorkine-Hornung, Daniel Cohen-Or, and Baoquan Chen. Skeleton-aware networks for deep motion retargeting. *ACM Transactions on Graphics (TOG)*, 39(4):62, 2020.
- [29] Jack M Wang, David J Fleet, and Aaron Hertzmann. Gaussian process dynamical models for human motion. *IEEE transactions on pattern analysis and machine intelligence*, 30(2):283–298, 2007.
- [30] Daniel Holden, Jun Saito, Taku Komura, and Thomas Joyce. Learning motion manifolds with convolutional autoencoders. In *SIGGRAPH Asia 2015 Technical Briefs*, page 18. ACM, 2015.

- [31] He Zhang, Sebastian Starke, Taku Komura, and Jun Saito. Mode-adaptive neural networks for quadruped motion control. *ACM Trans. Graph.*, 37(4), July 2018.
- [32] Sebastian Starke, He Zhang, Taku Komura, and Jun Saito. Neural state machine for character-scene interactions. *ACM Trans. Graph.*, 38(6), November 2019.
- [33] Jungdam Won, Deepak Gopinath, and Jessica Hodgins. A scalable approach to control diverse behaviors for physically simulated characters. *ACM Trans. Graph.*, 39(4), July 2020.
- [34] Sebastian Starke, Yiwei Zhao, Taku Komura, and Kazi Zaman. Local motion phases for learning multi-contact character movements. *ACM Trans. Graph.*, 39(4), July 2020.
- [35] Xue Bin Peng, Pieter Abbeel, Sergey Levine, and Michiel van de Panne. Deepmimic: Example-guided deep reinforcement learning of physics-based character skills. *ACM Transactions on Graphics (TOG)*, 37(4):143, 2018.
- [36] Ying-Sheng Luo, Jonathan Hans Soeseno, Trista Pei-Chun Chen, and Wei-Chao Chen. Carl: Controllable agent with reinforcement learning for quadruped locomotion. *ACM Transactions on Graphics (Proceedings of SIGGRAPH 2020)*, 39(4), 2020.
- [37] Libin Liu and Jessica Hodgins. Learning basketball dribbling skills using trajectory optimization and deep reinforcement learning. *ACM Trans. Graph.*, 37(4), July 2018.
- [38] Libin Liu and Jessica Hodgins. Learning to schedule control fragments for physics-based characters using deep q-learning. *ACM Trans. Graph.*, 36(3), June 2017.
- [39] Libin Liu, Michiel van de Panne, and KangKang Yin. Guided learning of control graphs for physics-based characters. *ACM Transactions on Graphics*, 35(3), 2016.
- [40] Xue Bin Peng, Glen Berseth, KangKang Yin, and Michiel Van De Panne. Deeploco: Dynamic locomotion skills using hierarchical deep reinforcement learning. *ACM Transactions on Graphics (TOG)*, 36(4):41, 2017.
- [41] Zhiyong Wang, Jinxiang Chai, and Shihong Xia. Combining recurrent neural networks and adversarial training for human motion synthesis and control. *IEEE Transactions on Visualization and Computer Graphics*, pages 1–1, 2019.
- [42] Omid Alemi, Jules Françoise, and Philippe Pasquier. Groovenet: Real-time music-driven dance movement generation using artificial neural networks. *networks*, 8(17):26, 2017.
- [43] Angela S Lin, Lemeng Wu, Rodolfo Corona, Kevin Tai, Qixing Huang, and Raymond J Mooney. Generating animated videos of human activities from natural language descriptions. In *NeurIPS*, 2018.
- [44] Ashesh Jain, Amir R Zamir, Silvio Savarese, and Ashutosh Saxena. Structural-rnn: Deep learning on spatio-temporal graphs. In *Proceedings of the IEEE Conference on Computer Vision and Pattern Recognition*, pages 5308–5317, 2016.
- [45] Qiang Nie, Ziwei Liu, and Yunhui Liu. Unsupervised 3d human pose representation with viewpoint and pose disentanglement. In *European Conference on Computer Vision (ECCV)*, 2020.
- [46] Enric Corona, Albert Pumarola, Guillem Alenya, and Francesc Moreno-Noguer. Context-aware human motion prediction. In *IEEE/CVF Conference on Computer Vision and Pattern Recognition (CVPR)*, June 2020.
- [47] Judith Butepage, Michael J Black, Danica Kragic, and Hedvig Kjellstrom. Deep representation learning for human motion prediction and classification. In *Proceedings of the IEEE conference on computer vision and pattern recognition*, pages 6158–6166, 2017.
- [48] Mao Wei, Liu Miaomiao, and Salzemann Mathieu. History repeats itself: Human motion prediction via motion attention. In *ECCV*, 2020.
- [49] Ye Yuan and Kris Kitani. Residual force control for agile human behavior imitation and extended motion synthesis. In *Advances in Neural Information Processing Systems*, 2020.
- [50] Jingwei Xu, Huazhe Xu, Bingbing Ni, Xiaokang Yang, Xiaolong Wang, and Trevor Darrell. Hierarchical style-based networks for motion synthesis. In *eccv*, 2020.
- [51] Maosen Li, Siheng Chen, Yangheng Zhao, Ya Zhang, Yanfeng Wang, and Qi Tian. Dynamic multiscale graph neural networks for 3d skeleton based human motion prediction. In *IEEE/CVF Conference on Computer Vision and Pattern Recognition (CVPR)*, June 2020.
- [52] Qiongjie Cui, Huaijiang Sun, and Fei Yang. Learning dynamic relationships for 3d human motion prediction. In *IEEE/CVF Conference on Computer Vision and Pattern Recognition (CVPR)*, June 2020.
- [53] Ruben Villegas, Jimei Yang, Duygu Ceylan, and Honglak Lee. Neural kinematic networks for unsupervised motion retargeting. In *Proceedings of the IEEE Conference on Computer Vision and Pattern Recognition*, pages 8639–8648, 2018.

- [54] Sadegh Aliakbarian, Fatemeh Sadat Saleh, Mathieu Salzmann, Lars Petersson, and Stephen Gould. A stochastic conditioning scheme for diverse human motion prediction. In *IEEE/CVF Conference on Computer Vision and Pattern Recognition (CVPR)*, June 2020.
- [55] Rui Zhao, Hui Su, and Qiang Ji. Bayesian adversarial human motion synthesis. In *IEEE/CVF Conference on Computer Vision and Pattern Recognition (CVPR)*, June 2020.
- [56] Zimo Li, Yi Zhou, Shuangjiu Xiao, Chong He, and Hao Li. Auto-conditioned lstm network for extended complex human motion synthesis. *arXiv preprint arXiv:1707.05363*, 3, 2017.
- [57] Dario Pavllo, David Grangier, and Michael Auli. Quaternion: A quaternion-based recurrent model for human motion. In *BMVC*, 2018.
- [58] Wikipedia. Quaternion — Wikipedia, the free encyclopedia, 2020. [Online; accessed 19-November-2020].
- [59] Alex Graves. Generating sequences with recurrent neural networks. *Computer Science*, 2013.
- [60] Xiaolin K. Wei, Peizhao Zhang, and Jinxiang Chai. Accurate realtime full-body motion capture using a single depth camera. *ACM Trans. Graph.*, 31(6):188:1–188:12, 2012.
- [61] Samuel R. Buss. Introduction to inverse kinematics with jacobian transpose, pseudoinverse and damped least squares methods. Technical report, IEEE Journal of Robotics and Automation, 2004.

8 Supplementary Material

8.1 Details of Network Parameters

CCNet: The detailed parameters of the separate dilation blocks (SRB) used in the CCNet are shown in Tab.8 and Tab.9 respectively. The format of the "output size" column is $\#channel \times \#NCF$, where $\#channel$ indicates the numbers of feature channels and $\#NCF$ indicates the number of consecutive frames (NCF) of each sample in a batch.

The modification of ERD-4LR and DAE-LSTM: Both original ERD-4LR and DAE-LSTM networks in Sec.6 of our paper have 1024 hidden units in the linear layers and 512 hidden units in the LSTM layers. To test the performance of these two types of networks in the multi-subject motion synthesis, we add additional parameters to let the network accept as inputs the skeleton configuration. Specifically, we add a Linear-Tanh module (with 1024 hidden units in the Linear layer) for ERD-4LR and DAE-LSTM to map skeleton configurations to features and then add them to the feature output by the encoder. The summed features are fed to LSTM layers for the random motion synthesis. We denote these two adapted networks for random motion synthesis as *ERD-4LR-rand* and *DAE-LSTM-rand*. Their network parameters are shown in Tab.10.

Similarly, to extend ERD-4LR and DAE-LSTM to support multi-subject, controllable motion synthesis, we additionally add a Linear-Tanh module (with 1024 hidden units in the Linear layer) to convert each of the control signals into features. Similarly, these features are added to the encoder output to form the input of subsequent LSTM layers. We denote the two adapted networks for controllable motion synthesis as *ERD-4LR-cond* and *DAE-LSTM-cond*. Their network parameters are shown in Tab.11.

The modification of PFNN: We also adapt the network architecture of PFNN [5] to take the skeleton configuration as an input. It is implemented by replacing terrain data in its original inputs with the skeleton configuration since we only test the synthesis of motions on a ground plane. The rest inputs of PFNN remain the same as in [5]. Since PFNN is mainly designed for controllable motion synthesis, not a generative model, we only compare the CCNet with PFNN on controllable motion synthesis. The modified PFNN is denoted as *PFNN-cond*, and its network parameters are shown in Tab.12.

8.2 Trajectory-following Error Comparisons

Fig.14 illustrates the six manually specified trajectories used in the trajectory-following error comparison of controllable motion synthesis (the "comparisons" paragraph in Sec. 6.2 in our paper). The trajectory-following error for all the trajectories is visualized in Fig.9.

8.3 User Study

Motion generation: To conduct the user study, we first randomly select 16 mocap sequences from the validation dataset, including five motion sequences of subject 7 and one motion sequence of each of the rest of subjects in our database. Since subject 7 is not included in the training dataset, we thus choose more number of its motions to check the motion quality, in this case, more carefully. Secondly, for the user study on random motion synthesis, we initialize the

	Source of Variation	SS	df	MS	F	P-value	F-critical
Random motion synthesis	Between Groups	171.375	2	85.6875	59.3792	2.3862e-13	3.2043
	Within Groups	64.9375	45	1.4431	-	-	-
	Total	236.3125	47	-	-	-	-
Controllable motion synthesis	Between Groups	346.6875	3	115.5625	90.342	3.1855e-22	2.7581
	Within Groups	76.75	60	1.2792	-	-	-
	Total	423.4375	63	-	-	-	-

Table 7: ANOVA-test of user study for confidence interval=0.95 in the cases of random and controllable motion synthesis. SS: sum-of-squares for between-group variability. Df: degrees of freedom. MS: mean squares. F: F ratio. -: not applicable.

CCNet and baseline models using the first 120 frames of each mocap sequence as seed frames. Consequently, we obtain 16 sequences generated by CCNet, ERD-4LR-rand, and DAE-LSTM-rand, respectively, to form three groups of motion pairs. For controllable motion synthesis, seed frames are the same 120 frames of each sequence, and control signals are extracted from the 16 mocap sequences as described in section 4.2. The extracted control signals guarantee that these networks generate motions with the same motion types as the mocap sequences. We apply CCNet, ERD-4LR-cond, DAE-LSTM-cond, and PFNN-cond to generate 16 motion sequences separately. The average length of selected motion sequences is around 10 seconds, and the length of each generated motion sequence is chosen to be the same length as the corresponding mocap sequence. All the motion sequence pairs are present to the participants in a random order for their evaluation.

We name the videos of the generated motion sequences as follows: "rand0" and "cond0" are used for the videos of mocap data; "rand1" and "cond1" for the videos of motions generated by the CCNet; "rand2" and "cond2" for ERD-4LR-rand and ERD-4LR-cond; "rand3" and "cond3" for DAE-LSTM-rand and DAE-LSTM-cond; and "cond4" for PFNN-cond.

ANOVA-test: We also perform an ANOVA-test on the user study results as illustrated in Tab.7, which also verifies the statistical significance of the user study.

Block name	Output size	Filter size
CausalConv1	32×240	1×1, 32, stride 1, dilation 2, padding (2, 0); input: motion frames
cond1_conv1+ReLU	32×240	1×1, 32, stride 1, padding 1, dilation 1; input: c1
cond2_conv1+ReLU	32×240	1×1, 32, stride 1, padding 1, dilation 1; input: c2
cond3_conv1+ReLU	32×240	1×1, 32, stride 1, padding 1, dilation 1; input: c3
CausalConv2	32×240	1×1, 32, stride 1, dilation 2, padding (2, 0); input: the same as it to CausalConv1
cond1_conv2+ReLU	32×240	1×1, 32, stride 1, padding 1, dilation 1; input: the same as it to cond1_conv1
cond2_conv2+ReLU	32×240	1×1, 32, stride 1, padding 1, dilation 1; input: the same as it to cond2_conv1
cond3_conv2+ReLU	32×240	1×1, 32, stride 1, padding 1, dilation 1; input: the same as it to cond3_conv1
sigmoid	32×240	input: the sum of CausalConv1, cond1_conv1+ReLU, cond2_conv1+ReLU and cond3_conv1+ReLU
Tanh	32×240	input: the sum of CausalConv2, cond1_conv2+ReLU, cond2_conv2+ReLU and cond3_conv2+ReLU
element-wise multiply	32×240	input: sigmoid and Tanh
conv_res	32×240	1×1, 32, stride 1, padding 1, dilation 1; input: element-wise multiply output(SRB_resi): the sum of conv_res and the input to CausalConv1
conv_skip	512×240	1×1, 512, stride 1, padding 1, dilation 1; input: element-wise multiply output(SRB_skipi): the output of conv_skip

Table 8: Network parameters of a single SRB_i. The dilation of SRB_i is 2.

Block name	Output size	Filter size
Encoder		
conv1+ReLU	32×240	1×1, 32, stride 1, padding 1, dilation 1
conv2+ReLU	32×240	1×1, 32, stride 1, padding 1, dilation 1
Separate Residual Blocks(SRBs)		
SRB0	SRB_res0: 32×240	dilation 2; input: conv2, c1, c2 and c3
	SRB_skip0: 512×240	dilation 2; input: conv2, c1, c2 and c3
SRB1	SRB_res1: 32×240	dilation 2; input: SRB_res0, c1, c2 and c3
	SRB_skip1: 512×240	dilation 2; input: SRB_res0, c1, c2 and c3
SRB2	SRB_res2: 32×240	dilation 2; input: SRB_res1, c1, c2 and c3
	SRB_skip2: 512×240	dilation 2; input: SRB_res1, c1, c2 and c3
SRB3	SRB_res3: 32×240	dilation 2; input: SRB_res2, c1, c2 and c3
	SRB_skip3: 512×240	dilation 2; input: SRB_res2, c1, c2 and c3
SRB4	SRB_res4: 32×240	dilation 2; input: SRB_res3, c1, c2 and c3
	SRB_skip4: 512×240	dilation 2; input: SRB_res3, c1, c2 and c3
SRB5	SRB_res5: 32×240	dilation 2; input: SRB_res4, c1, c2 and c3
	SRB_skip5: 512×240	dilation 2; input: SRB_res4, c1, c2 and c3
SRB6	SRB_res6: 32×240	dilation 2; input: SRB_res5, c1, c2 and c3
	SRB_skip6: 512×240	dilation 2; input: SRB_res5, c1, c2 and c3
SRB7	SRB_res7: 32×240	dilation 2; input: SRB_res6, c1, c2 and c3
	SRB_skip7: 512×240	dilation 2; input: SRB_res6, c1, c2 and c3
SRB8	SRB_res8: 32×240	dilation 2; input: SRB_res7, c1, c2 and c3
	SRB_skip8: 512×240	dilation 2; input: SRB_res7, c1, c2 and c3
SRB9	SRB_res9: 32×240	dilation 2; input: SRB_res8, c1, c2 and c3
	SRB_skip9: 512×240	dilation 2; input: SRB_res8, c1, c2 and c3
SRB10	SRB_res10: 32×240	dilation 2; input: SRB_res9, c1, c2 and c3
	SRB_skip10: 512×240	dilation 2; input: SRB_res9, c1, c2 and c3
SRB11	SRB_res11: 32×240	dilation 2; input: SRB_res10, c1, c2 and c3
	SRB_skip11: 512×240	dilation 2; input: SRB_res10, c1, c2 and c3
SRB12	SRB_res12: 32×240	dilation 2; input: SRB_res11, c1, c2 and c3
	SRB_skip12: 512×240	dilation 2; input: SRB_res11, c1, c2 and c3
SRB13	SRB_res13: 32×240	dilation 2; input: SRB_res12, c1, c2 and c3
	SRB_skip13: 512×240	dilation 2; input: SRB_res12, c1, c2 and c3
SRB14	SRB_res14: 512×240	dilation 2; input: SRB_res13, c1, c2 and c3
Decoder		
ReLU+conv3	512×240	1×1, 512, stride 1, padding 1, dilation 1; input: the sum of SRB_skip0, SRB_skip1, ..., SRB_skip14
ReLU+conv4	613×240	1×1, 613, stride 1, padding 1, dilation 1

Table 9: Network parameters of the CCNet. The input to the CCNet includes 240 frames of motions, the skeleton configuration c1, the direction and velocity c2, and the motion type c3. The network architecture of the CCNet is inspired by [8].

Block name	Output size	Input/Output
linear1+Tanh	1024×240	input: motion frames output: linear1
linear2+Tanh	1024×240	input: linear1 output: linear2
cond1_linear+Tanh	1024×240	input: c1 output: cond1_linear
cond2_linear+Tanh	1024×240	input: c2 output: cond2_linear
cond3_linear+Tanh	1024×240	input: c3 output: cond3_linear
LSTM1	512×240	input: the sum of the linear2, cond_linear1, cond_linear2 and cond_linear3 output: lstm1
LSTM2	512×240	input: lstm1 output: lstm2
LSTM3	512×240	input: lstm2 output: lstm3
LSTM4	1024×240	input: lstm3 output: lstm4
linear3+Tanh	1024×240	input: lstm4 output: linear3
linear4+Tanh	613×240	input: linear3 output: the predicted motion frames

(a) ERD-4LR-rand.

Block name	Output size	Input/Output
linear1+Tanh	1024×240	input: motion frames output: linear1
linear2+Tanh	1024×240	input: linear1 output: linear2
cond1_linear+Tanh	1024×240	input: c1 output: cond1_linear
cond2_linear+Tanh	1024×240	input: c2 output: cond2_linear
cond3_linear+Tanh	1024×240	input: c3 output: cond3_linear
LSTM1	512×240	input: the sum of the linear2, cond_linear1, cond_linear2 and cond_linear3 output: lstm1
LSTM2	512×240	input: lstm1 output: lstm2
LSTM3	512×240	input: lstm2 output: lstm3
LSTM4	1024×240	input: lstm3 output: lstm4
linear3+Tanh	1024×240	input: lstm4 output: linear3
linear4+Tanh	613×240	input: linear3 output: the predicted motion frames

(b) ERD-4LR-cond.

Table 10: Network parameters of the ERD-4LR-rand and ERD-4LR-cond. The inputs to the ERD-4LR-rand and ERD-4LR-cond include 240 frames of motions, the skeleton configuration c1, the direction and velocity c2, and the motion type c3. The overall network architectures of ERD-4LR-rand and ERD-4LR-cond are the adaptation of [2] to multi-subject motion synthesis, but implemented with 4-layers LSTM as in [6].

Block name	Output size	Input/Output
dropout+linear1+ReLU	1024×240	dropout probability: 0.3 input: motion frames output: linear1
linear2+ReLU	1024×240	input: linear1 output: linear2
linear3+ReLU	1024×240	input: linear2 output: linear3
linear4	305×240	input: linear3 output: linear4
LSTM1	512×240	input: linear2, output: lstm1
LSTM2	512×240	input: lstm1 output: lstm2
LSTM3	512×240	input: lstm2 output: lstm3
linear5	613×240	input: lstm3 output: the predicted motion frames

(a) DAE-LSTM-rand.

Block name	Output size	Input/Output
dropout+linear1+ReLU	1024×240	dropout probability: 0.3 input: motion frames output: linear1
linear2+ReLU	1024×240	input: linear1 output: linear2
linear3+ReLU	1024×240	input: linear2 output: linear3
linear4	305×240	input: linear3 output: linear4
cond1_linear+Tanh	1024×240	input: c1 output: cond1_linear
cond2_linear+Tanh	1024×240	input: c2 output: cond2_linear
cond3_linear+Tanh	1024×240	input: c3 output: cond3_linear
LSTM1	512×240	input: the sum of the linear4, cond_linear1, cond_linear2 and cond_linear3 output: lstm1
LSTM2	512×240	input: lstm1 output: lstm2
LSTM3	512×240	input: lstm2 output: lstm3
linear5	613×240	input: lstm3 output: the predicted motion frames

(b) DAE-LSTM-cond.

Table 11: Network parameters of DAE-LSTM-rand and DAE-LSTM-cond. The inputs to the DAE-LSTM-rand and DAE-LSTM-cond include 240 frames of motions, the skeleton configuration c1, the direction and velocity c2, and the motion type c3. The overall network architectures of DAE-LSTM-rand and DAE-LSTM-cond are the adaptation of the network in [25] to multi-subject motion synthesis.

Block name	Output size	Input/Output
dropout+pfnn_linear1+ELU	512×1	dropout probability: 0.7 input: the concatenation of motion frames and control signals output: pfnn_linear1
dropout+pfnn_linear2+ELU	512×1	dropout probability: 0.7 input: pfnn_linear1 output: pfnn_linear2
dropout+pfnn_linear3	437×1	dropout probability: 0.7 input: pfnn_linear2 output: the predicted motion frames and control signals

Table 12: Network parameters of the PFNN-cond. The input to the PFNN-cond is described in Sec.1 in the supplementary material.

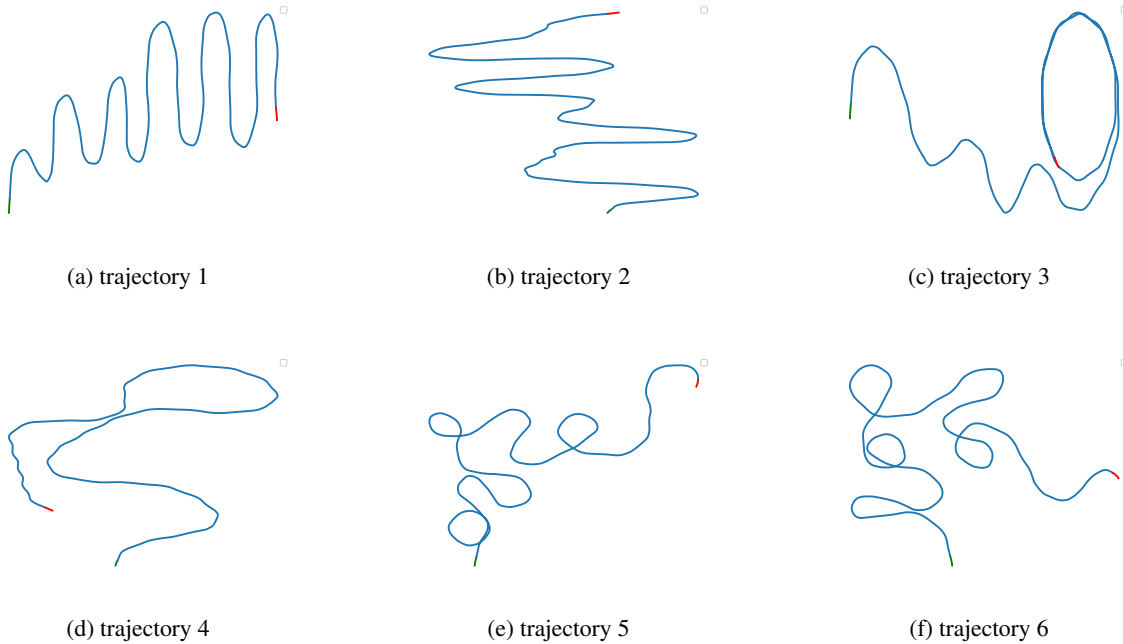


Figure 14: Six trajectories used in trajectory-following comparisons. The green color indicates the starting point of a trajectory, while the red color indicates the terminal point.